



# Biomimetic gradient scaffold of collagen–hydroxyapatite for osteochondral regeneration

Journal of Tissue Engineering  
Volume 11: 1–13  
© The Author(s) 2020  
Article reuse guidelines:  
[sagepub.com/journals-permissions](https://sagepub.com/journals-permissions)  
DOI: 10.1177/2041731419896068  
[journals.sagepub.com/home/tej](https://journals.sagepub.com/home/tej)



Cristian Parisi<sup>1,2</sup>, Luca Salvatore<sup>2</sup>, Lorenzo Veschini<sup>1</sup>,  
Maria Paola Serra<sup>3,4</sup>, Carl Hobbs<sup>5</sup>, Marta Madaghiele<sup>2</sup>,  
Alessandro Sannino<sup>2</sup> and Lucy Di Silvio<sup>1</sup>

## Abstract

Osteochondral defects remain a major clinical challenge mainly due to the combined damage to the articular cartilage and the underlying bone, and the interface between the two tissues having very different properties. Current treatment modalities have several limitations and drawbacks, with limited capacity of restoration; however, tissue engineering shows promise in improving the clinical outcomes of osteochondral defects. In this study, a novel gradient scaffold has been fabricated, implementing a gradient structure in the design to mimic the anatomical, biological and physicochemical properties of bone and cartilage as closely as possible. Compared with the commonly studied multi-layer scaffolds, the gradient scaffold has the potential to induce a smooth transition between cartilage and bone and avoid any instability at the interface, mimicking the natural structure of the osteochondral tissue. The scaffold comprises a collagen matrix with a gradient distribution of low-crystalline hydroxyapatite particles. Physicochemical analyses confirmed phase and chemical compositions of the gradient scaffold and the distribution of the mineral phase along the gradient scaffold. Mechanical tests confirmed the gradient of stiffness throughout the scaffold, according to its mineral content. The gradient scaffold exhibited good biological performances both *in vitro* and *in vivo*. Biological evaluation of the scaffold, in combination with human bone-marrow–derived mesenchymal stem cells, demonstrated that the gradient of composition and stiffness preferentially increased cell proliferation in different sub-regions of the scaffold, according to their high chondrogenic or osteogenic characteristics. The *in vivo* biocompatibility of the gradient scaffold was confirmed by its subcutaneous implantation in rats. The gradient scaffold was significantly colonised by host cells and minimal foreign body reaction was observed. The scaffold's favourable chemical, physical and biological properties demonstrated that it has good potential as an engineered osteochondral analogue for the regeneration of damaged tissue.

## Keywords

Collagen, hydroxyapatite, tissue engineering, cartilage, bone

Date received: 27 July 2019; accepted: 29 November 2019

<sup>1</sup>Centre of Oral, Clinical & Translational Sciences, King's College London, London, UK

<sup>2</sup>Department of Engineering for Innovation, University of Salento, Lecce, Italy

<sup>3</sup>Centre for Stem Cells & Regenerative Medicine, King's College London, London, UK

<sup>4</sup>Department of Biomedical Sciences, University of Cagliari, Cagliari, Italy

<sup>5</sup>Wolfson Centre for Age-Related Diseases, King's College London, London, UK

## Corresponding authors:

Cristian Parisi, Centre of Oral, Clinical & Translational Sciences, King's College London, London SE1 9RT, UK.  
Email: [cristian.parisi1@gmail.com](mailto:cristian.parisi1@gmail.com)

Lucy Di Silvio, Centre of Oral, Clinical & Translational Sciences, King's College London, London SE1 9RT, UK.  
Email: [lucy.di\\_silvio@kcl.ac.uk](mailto:lucy.di_silvio@kcl.ac.uk)



## Introduction

Articular cartilage has no innate ability to repair when damaged due to its avascular nature, and lacks a rich source of progenitor cells and growth factors required for regeneration.<sup>1</sup> Although a number of therapeutic approaches have been proposed to treat osteochondral defects, none to date has been proven to ensure a sustained regeneration. Current clinical approaches have shown significant limitations and drawbacks, and offer mostly temporary reduction in the symptoms without any repair of the damaged tissues.<sup>2</sup>

The difficulties encountered are mostly dependent on the intrinsic biological, biochemical and biomechanical properties of the articular cartilage.

Repair of osteochondral defects by tissue engineering, therefore, offers a more biological approach mimicking the natural tissue and more effective methods for the treatment of osteochondral defects.<sup>3</sup> Numerous studies have reported multi-layer scaffolds, where two or more different phases are arranged to create discrete, non-continuous layers to replicate cartilage and bone sub-regions of the osteochondral structure. In some studies, a further layer was added as an interface-like sub-region.<sup>4–6</sup> Although multi-layer scaffolds showed good properties and some potential for their use in osteochondral regeneration, they do not mimic closely enough the unique gradient structure of the natural tissue, often showing instability at the interface between soft and hard tissue.<sup>3</sup> Moreover, fabrication techniques often involve several freeze-drying steps or further processing to assure an adequate adhesion of the various layers, highlighting their technical and economical limitations.<sup>6</sup>

In the human body, gradients are observed between tissues, mostly connecting tissues of different properties, for example, the osteochondral tissue. This tissue is characterised by a gradual transition from hard mineralised subchondral bone to hyaline cartilage immediately above it. The natural tissue is not simply a multi-layer structure, but a continuum of viscoelastic-soft articular cartilage which develops in an underlying stiff vascularised bone tissue.<sup>7</sup> Hence, in designing and fabricating interfacing scaffolds, the major challenge is to mimic the anatomical, biological and physicochemical properties of the natural tissue.<sup>3,7</sup> However, there are few studies reported in the literature describing gradient scaffolds for osteochondral regeneration, and most are still at a very preliminary experimental stage.<sup>3,8–13</sup> Hence, there is still an unmet clinical and scientific need for an improved approach for the treatment of osteochondral defects.<sup>6</sup>

The aim of this study was to design and fabricate a highly porous, integrative and cell-instructive scaffold, using a continuum model and selected biomaterials to fulfil the necessary features of the complex osteochondral tissue interface. The scaffold's physicochemical properties were fully characterised. In vitro tests were performed using a human bone-marrow-derived mesenchymal stem

cells (hBMSCs) model to assess the specificity of cellular response to the different regions of the gradient scaffold. In vivo biocompatibility was tested in a rat model.

## Materials and methods

### *Fabrication of the gradient scaffold*

A water-soluble bovine type I collagen (Symatase Biomaterialux, France) was used as the collagen source. Calcium hydroxide,  $\text{Ca}(\text{OH})_2$ , and phosphoric acid ( $\text{H}_3\text{PO}_4$ ; Sigma Aldrich, St. Louis, MI, USA), were used as, respectively, calcium and phosphate precursors for the synthesis of hydroxyapatite particles. Hydroxyapatite/collagen (HAp/Coll) composite aqueous suspensions (slurries) were synthesised with four different weight ratios as follows: 0/100, 10/90, 30/70 and 50/50. The pure collagen slurry (HAp/Coll 0/100) was prepared by adding 3 g of collagen to 100 mL of distilled water. For the HAp/Coll 10/90 synthesis, 0.246 g of  $\text{Ca}(\text{OH})_2$  was sonicated in 50 mL of distilled water for 5 min to obtain a homogeneous suspension. Then, 3 g of collagen was added in the suspension and vigorously stirred at a constant temperature of 10°C for 3 h to obtain a homogeneous collagen slurry. Following this, 50 mL of a  $\text{H}_3\text{PO}_4$  aqueous solution (0.230 g of 85%  $\text{H}_3\text{PO}_4$ ) was added drop-wise to the  $\text{Ca}(\text{OH})_2$ /Coll suspension while stirring. Co-precipitation of HAp particles onto the collagen fibres occurred during this phase. The HAp/Coll 30/70 and 50/50 composite slurries were prepared following the same protocol, but changing the initial concentration of calcium and phosphorous precursors, according to the desired weight ratio. The Ca/P molar ratio for all the suspensions was 1.67, which is the stoichiometric value for pure HAp.

The gradient scaffold was obtained by a combination of all the four composite aqueous suspensions using a sequential addition technique. Slurries were pipetted into cylindrical moulds (9 mm diameter and 10 mm height), starting from the slurry with the highest HAp content, the HAp/Coll 50/50 slurry, followed by a decreasing HAp content up to the pure collagen slurry (HAp/Coll 0/100) (Figure 1). In this way, the sub-region at the bottom of the scaffold contained the highest HAp content, therefore was considered to represent the bone-like region of the gradient scaffold. The immediate region above the bone-like one was designated as the lower middle zone, then the upper middle zone and, at the top, the cartilage-like region (Figure 1). The thickness of each sub-region was tailored by simply changing the pipetted volume of each slurry. A highly porous structure was obtained by a standard one-step freeze-drying process (Advantage EL Freeze-dryer, VirTis Co., Gardiner, NY, USA) of the slurries, previously pipetted into the mould.

### *Crosslink and sterilisation of the scaffold*

After freeze-drying, scaffolds were crosslinked using a standard dehydrothermal treatment (DHT) in a vacuum

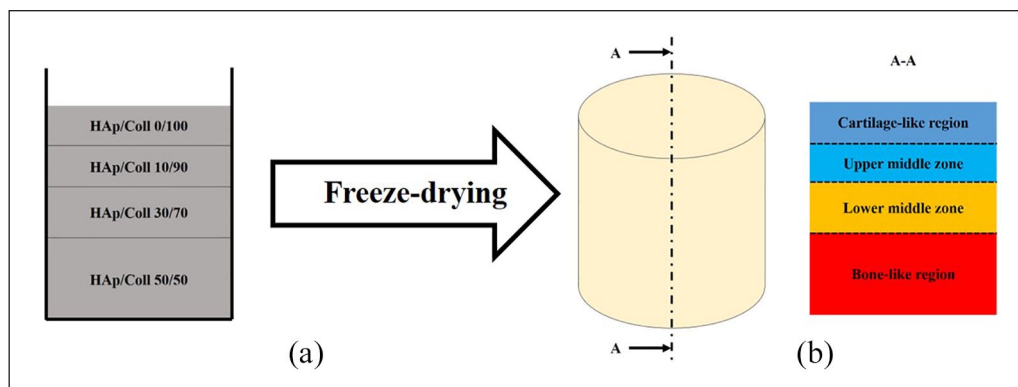


**Figure 1.** (a) Slurries pipetted in a sequence into the mould to obtain the gradient structure, and (b) after freeze-drying the approximate zone sizes of its main sub-regions, from the cartilage-like region to the bone-like region.

oven (100 mTorr) at 121°C for 48 h.<sup>14,15</sup> This treatment was then followed by a chemical crosslinking process, carried out using a water-soluble carbodiimide, 1-ethyl-3-(3-dimethylaminopropyl) carbodiimide (EDC, Sigma Aldrich), and N-hydroxysuccinimide (NHS, Sigma Aldrich), following a well-established protocol.<sup>16,17</sup> After a final freeze-drying process, all the samples were ultimately sterilised under vacuum (100 mTorr) at 165°C for a period of 3 h, according to a standard dehydrothermal sterilisation (DHS) protocol.

### Physicochemical analysis

The phase composition of the gradient scaffold was verified by X-ray diffraction (XRD) analyses (D/Max Ultima Diffractometer, Rigaku, Japan). This technique was used to detect and characterise crystalline or semi-crystalline phases within the scaffold and to verify the presence of HAp inside the scaffold and to exclude the presence of other mineral phases. XRD patterns ( $n=3$ ) were obtained with  $\text{CuK}\alpha$  radiation ( $\lambda=0.15418$  nm) in step scanning mode recorded in the  $2\theta$  range of 20°–80°, with a step size of 0.02° and step duration of 0.5 s. Patterns were then analysed referring to the database for XRD analyses of the International Centre for Diffraction Data (former Joint Committee on Powder Diffraction Standards; ICDD-JCPDS).<sup>18</sup>

The chemical composition of the gradient scaffold was analysed using Fourier transform infrared (FTIR) spectroscopy by an attenuated total reflectance (ATR) spectrometer (Spectrum One; Perkin Elmer, Waltham, MA, USA). Spectra of each sub-region ( $n=3$ ) of the scaffold were analysed and compared with pure collagen I and pure HAp typical spectra,<sup>15,18</sup> to verify and confirm the presence and the distribution of those materials throughout each sub-region of the gradient scaffold and their chemical interaction.

Scanning electron microscopy (SEM) analyses were performed using an environmental SEM (Evo 50 XVP, Zeiss, Germany) with an accelerating voltage of 20 kV. These analyses were used to evaluate microstructural morphology, distribution of HAp particles and pores shapes,

sizes and distribution in each sub-region of the gradient scaffold. Each specimen ( $n=3$ ) was cut along its longitudinal axis to analyse the internal section of the scaffold. The entire section was analysed starting from the top cartilage-like region of the gradient scaffold, down to the bone-like region. SEM micrographs were taken at two different magnifications: 250× and 750×.

SEM analyses were coupled with energy-dispersive spectroscopy (EDS/EDX) to verify the distribution of Ca atoms in the collagen matrix and the atomic ratio between calcium and phosphorus atoms (Ca/P). In particular, the distribution of calcium atoms was assumed as the distribution of HAp particles throughout the gradient scaffold. Various areas ( $n=3$ ) of the scaffold, from the cartilage-like region to the bone-like region, were scanned using the SEM equipped with an EDS detector (Quantas XFlash<sup>®</sup> 6; Bruker, Billerica, MA, USA). The presence of calcium, phosphorus and carbon atoms was verified and their quantities were calculated by the machine software.

The mechanical behaviour of the gradient scaffold and each sub-region was evaluated by uniaxial unconfined compression tests using a universal testing machine (5569A; Instron, Norwood, MA, USA), equipped with a 10-N load cell at a crosshead speed of 0.05 mm/min.<sup>16,19</sup> Cylindrical specimens ( $n=6$ ), with a diameter of 8 mm and a height of 8 mm, were hydrated in Dulbecco's Modified Eagle Medium (DMEM, Sigma Aldrich) for 24 h prior to testing. For the mechanical characterisation of each sub-region of the gradient scaffold, individual layers of the appropriate concentration were prepared. Each specimen was then positioned at the centre of an empty Petri dish ( $d=60$  mm) on the fixed plate at the base of the machine for the test. After the application of a pre-load of 0.05 N, DMEM was flooded into the dish and the specimen was kept immersed throughout the test at room temperature. The compressive modulus was calculated via linear regression of the initial elastic domain of the obtained engineering stress ( $F/A_0$ ) versus engineering strain ( $\Delta L/L_0$ ) curve, between the engineering strain values of 0.02 and 0.1.<sup>16,19</sup>  $F$  (mN) is the applied load,  $A_0$  (mm<sup>2</sup>) is

the initial value of the cross-sectional area of the specimen,  $\Delta L$  (mm) is the displacement and  $L_0$  (mm) is the initial height of the specimen.

### Biological evaluation with hBMSCs

A preliminary *in vitro* evaluation of the biological performance of the gradient scaffold was carried out using a hBMSCs model. The ability of the scaffold to support hBMSCs viability and proliferation for both osteogenic and chondrogenic lineages was investigated. Each sub-region of the gradient scaffold was seeded with hBMSCs (Lonza, Basel, Switzerland). The constructs were seeded at a cell density of  $2.5 \times 10^5$  cells/scaffold and then cultured with osteogenic or chondrogenic differentiation medium to monitor cell viability and activity in both physiological media conditions. The osteogenic differentiation medium was prepared in low-glucose DMEM (D6046, Sigma Aldrich) supplemented with 10% foetal bovine serum (FBS), 1% penicillin–streptomycin (Pen/Strep),  $10^{-2}$ M  $\beta$ -glycerolphosphate (G9891, Sigma Aldrich),  $10^{-7}$ M dexamethasone (D2015, Sigma Aldrich) and 150  $\mu$ g/mL ascorbic acid (A4544, Sigma Aldrich). The chondrogenic differentiation medium was prepared in low-glucose DMEM (D6046, Sigma Aldrich) supplemented with 10% FBS, 1% Pen/Strep,  $10^{-8}$ M dexamethasone (D2015, Sigma Aldrich), 37  $\mu$ g/mL ascorbic acid (A4544, Sigma Aldrich), 1% ITS (human insulin, human transferrin and sodium selenite, I3146 Sigma Aldrich) and 10 ng/mL transforming growth factor  $\beta$ 3 (TGF- $\beta$ 3).

Considering the gradient scaffold design, the hypothesis of this experiment was that the lower middle zone and the bone-like region, characterised by the highest content of osteoconductive HAp, were expected to have a high potential to allow and favour cell viability and proliferation when conditioned in osteogenic medium.<sup>20,21</sup> Similarly, the cartilage-like region and the upper middle zone, characterised by a lower stiffness and a higher content of collagen, were expected to have a higher potential to allow and favour cell viability and proliferation when conditioned in chondrogenic medium.<sup>22</sup> Hence, hBMSCs seeded on lower middle zone and bone-like region of the gradient scaffold were conditioned in osteogenic medium and hBMSCs seeded on cartilage-like region and upper middle zone were conditioned in chondrogenic medium. The upper middle zone was chosen as the osteogenic control region and the lower middle zone was chosen as the chondrogenic control region, since these were representative of the subchondral bone interface.

hBMSCs exposed to chondrogenic or osteogenic medium in the sub-regions of the gradient scaffold were assessed for proliferation using alamarBlue™ assay (Thermo Fisher, Waltham, MA, USA).<sup>23–25</sup> At days 1, 7, 14, 21 and 28, differentiation media were replaced with 1 mL of alamarBlue solution (10% (v/v) alamarBlue in phenol red-free stem medium), then the plate was incubated at 37°C for 4 h. The solution was transferred to a 96-well plate in three technical replicates of 100  $\mu$ L each

for each sample ( $n=4$ ) and the absorbance at 570 nm was measured using a spectrophotometer (Opsys MR; Dynex Technologies, Chantilly, VA, USA).

### *In vivo* study

An *in vivo* evaluation of the biocompatibility of the gradient scaffold was carried out using a rat model. The study was conducted in accordance with the European Union Directive 2010/63/EU, with approval by the Ethics Committee for Animal Experimentation of the University of Cagliari (Italy). The model used for the study was 12-week-old female Fischer 344 rats ( $n=6$ ), with an average weight of 245 g. Prior to surgery, the animals were given general anaesthesia with isoflurane (1.5%) mixed with pure oxygen. When the animal was no longer responsive, an approximately 15-mm-long skin incision was made along the sagittal plane in the centre of the back of the animal and one cylindrical gradient scaffold was then implanted subcutaneously in each rat ( $n=6$ ). The incision was sutured using commercial bioresorbable sutures (Vicryl 5-0; Ethicon, Dülmen, Germany). Throughout the surgical procedure, due care was taken to minimise animal pain and discomfort. After 15 days, animals were euthanised and gradient scaffold along with approximately 5-mm-thick surrounding tissue were explanted from each rat and fixed in 10% formalin for 24 h at room temperature.

Cell colonisation of the gradient scaffold *in vivo* and cell distribution inside the scaffolds were analysed. After fixation, explanted scaffolds and surrounding tissues were first decalcified in ethylenediaminetetraacetic acid (EDTA) for 48 h and then processed and embedded in paraffin wax for histology. Slices of 10- $\mu$ m thickness were cut and mounted on microscopic slides and stained with haematoxylin and eosin (H&E). Immunohistochemistry was performed to identify potential proteins associated with differentiation; these included osteopontin (OPN), myocyte enhancer factor 2C (MEF2C) and haematoxylin–Van Geison (HVG).

### Statistical analysis

Results are reported as mean  $\pm$  standard deviation (SD). Statistical significance was predetermined at  $\alpha=0.05$  ( $p < \alpha$ ). One- and two-way analyses of variance (ANOVAs) were used to compare mean values among groups. A multiple comparison procedure, Tukey's test, was used to isolate the group or the groups that differed from the others. The following symbols are used to highlight statistical significance: \* $p < 0.05$ , \*\* $p < 0.01$  and \*\*\* $p < 0.001$ .

## Results

### Physicochemical properties

The gradient scaffold was successfully fabricated and appeared macroscopically homogeneous, with no evidenced

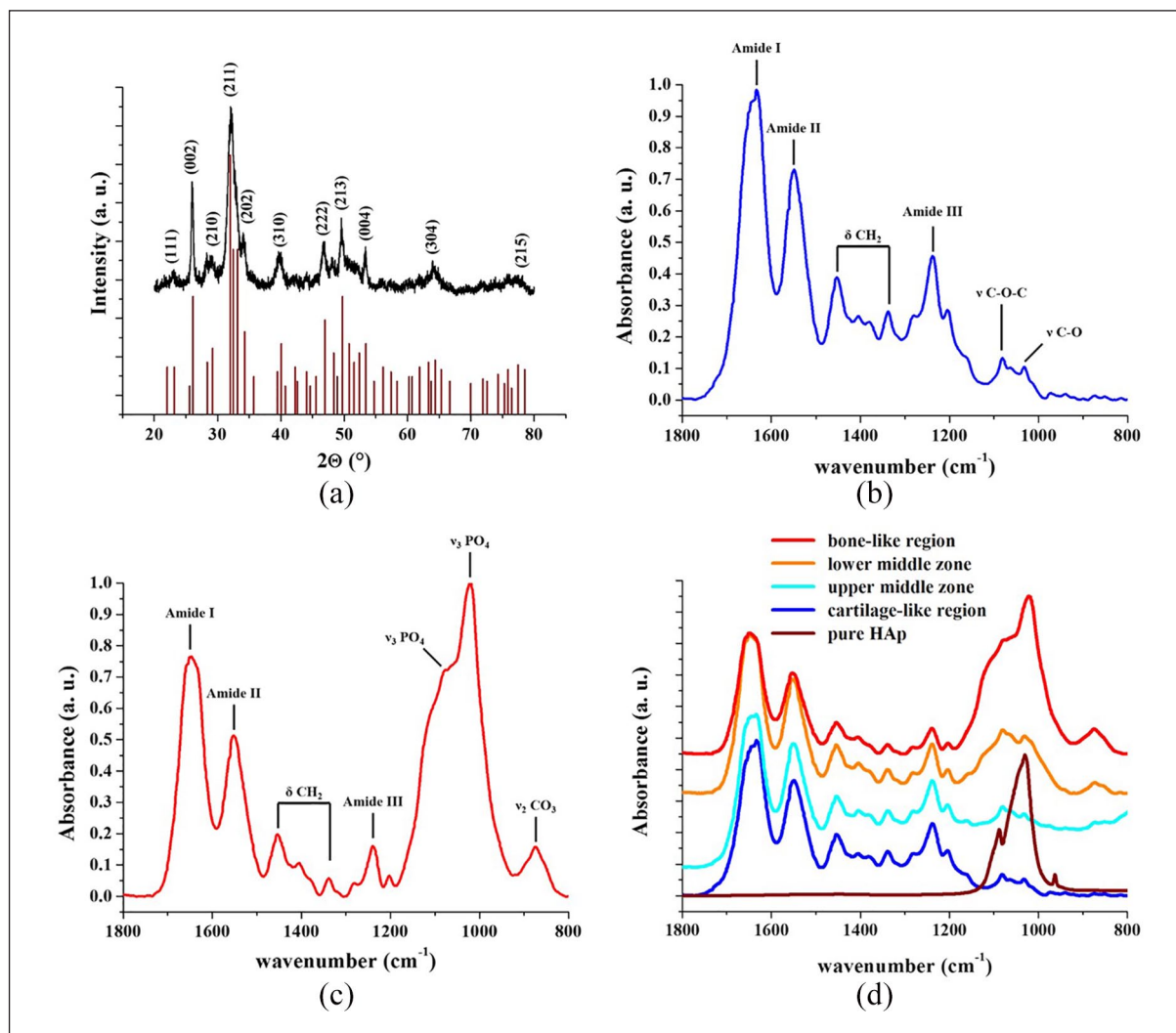


**Figure 2.** (a) A representative XRD pattern of the gradient HAP/Coll scaffold (black) compared with the XRD reference of HAP (brown; Ref. ICDD-JCPDS 09-0432). A low-crystalline HAP was the only mineral phase detected. (b) FTIR spectrum of the cartilage-like region of the gradient scaffold between 1800 and  $800 \text{ cm}^{-1}$ . (c) FTIR spectrum of the bone-like region of the gradient scaffolds with characteristic collagen and HAP peaks between 1800 and  $800 \text{ cm}^{-1}$ . The detection of the carbonate stretching at  $874 \text{ cm}^{-1}$  ( $\nu_2 \text{CO}_3$ ) confirmed the nucleation of the HAP particles onto the collagen fibres, chemically integrated with each other. (d) Comparison among the FTIR spectra of pure HAP (brown), cartilage-like region (blue), upper middle zone (light blue), lower middle zone (orange) and bone-like region (red) of the gradient scaffold between 1800 and  $800 \text{ cm}^{-1}$ .

separation at the interfaces. Figure 2(a) shows that the XRD pattern of the gradient scaffolds was comparable with the XRD reference of HAP (Ref. ICDD-JCPDS 09-0432). All the main peaks of pure HAP were detected, without any peaks of other phases of calcium phosphates.<sup>18,26</sup> The gradient scaffold exhibited broad diffraction peaks, indicating that the HAP particles, nucleated onto the collagen fibres, had a low crystallinity.<sup>27</sup>

In Figure 2(b), the typical pure collagen I absorption bands are highlighted in the spectra of the cartilage-like region of the scaffold between 1800 and  $800 \text{ cm}^{-1}$ . C=O stretching (amide I), N-H in-plane bending + C-N stretching (amide II),  $\text{CH}_2$  deformation ( $\delta \text{CH}_2$ ), C-N stretching + N-H in-plane bending (amide III), C-O-C stretching

( $\nu \text{C-O-C}$ ) and C-O stretching ( $\nu \text{C-O}$ ) were clearly detected.<sup>15</sup> The spectrum of the bone-like region of the gradient scaffold (Figure 2(c)) was analysed considering both pure collagen I<sup>15</sup> and pure HAP<sup>18,28,29</sup> characteristic absorption bands. All the main characteristic absorption peaks of collagen and HAP were clearly detected. The typical collagen C-O-C stretching ( $\nu \text{C-O-C}$ ) at  $1082 \text{ cm}^{-1}$  and C-O stretching ( $\nu \text{C-O}$ ) at  $1032 \text{ cm}^{-1}$  were covered by the stronger  $\text{PO}_4$  stretching ( $\nu_3 \text{PO}_4$ ) at  $1078$  and  $1020 \text{ cm}^{-1}$  due to the high HAP content.<sup>28,29</sup> This phenomenon was weaker in the lower middle zone (Figure 2(d), orange spectrum) because of a lower HAP content. The HAP content in the upper middle zone of the scaffold (Figure 2(d), light blue spectrum) was even lower and that impeded to detect any characteristic

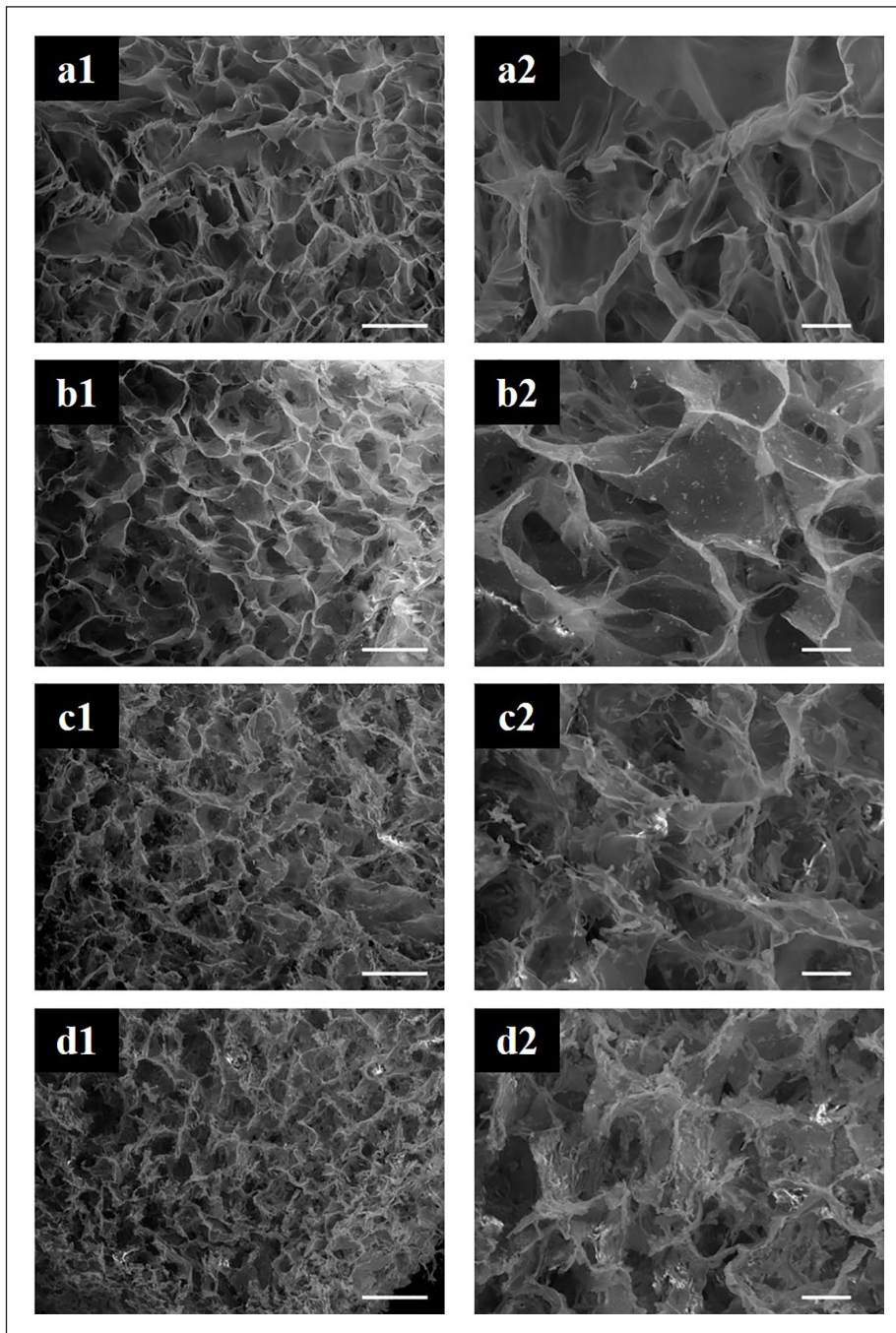


**Figure 3.** SEM micrographs of the different sub-regions of the gradient scaffold. The gradient distribution of the HAp particles in the highly porous collagen matrix was confirmed. Scale bars: (a1–d1) 200  $\mu\text{m}$  and (a2–d2) 50  $\mu\text{m}$ .

peak of HAp, showing only the typical absorption bands of collagen, similar to the cartilage-like region of the scaffold.

A clear confirmation of the chemical bond between collagen fibres and HAp was given by the detection of the characteristic peak of carbonate stretching at  $874\text{ cm}^{-1}$  ( $\nu_2$   $\text{CO}_3$ ) in the spectrum of the bone-like region of the gradient scaffold (Figure 2(c)). A weaker absorption was also found in the spectrum of the middle zone (Figure 2(d),

orange spectrum). This bond vibration is typical of carbonate apatite of mineralised collagen, confirming the nucleation of the mineral HAp particles onto the collagen fibres, chemically integrated with each other.<sup>30</sup> The amide III peak also showed a significantly lower intensity, as typically reported in the case of mineralised collagen.<sup>31</sup>

SEM micrographs in Figure 3 showed that the construct was overall highly porous with an open and interconnected

porosity. The concentration of HAp particles in the collagen matrix increased progressively from the cartilage-like region to the bone-like region, where the concentration was the highest. The first HAp particles were found in the upper middle zone of the scaffold (Figure 3). The concentration of the HAp particles increased progressively in the lower regions. The presence of HAp did not significantly change shape and distribution of the pores. It was clear how the presence of HAp particles increased the roughness of the surface of pores walls, comparing, in particular, cartilage-like and bone-like regions of the gradient scaffold.

EDS analysis showed that the ratio between calcium and carbon atoms increased progressively from the cartilage-like region to the bone-like region (Figure 4). This ratio was considered equivalent to the ratio of HAp and collagen, since no other chemical species were detected in the previous physicochemical analyses. Hence, this result clearly confirmed the gradient distribution of the mineral content throughout the scaffold.

An example of the engineering stress versus engineering strain curve obtained for each specimen of each sub-region and of the entire gradient scaffold is shown in Figure 5(a), that is, the typical mechanical response in compression expected from a low-density, elastomeric, open-cell and highly porous matrix.<sup>16</sup> The engineering stress versus engineering strain curve was characterised by the three distinct regimes, typical of this class of materials:

1. Linear elastic, mainly controlled by the bending of pores strut;
2. Collapse, with pores struts buckling and pores collapse – stress increases slightly;

3. Densification, where pores completely collapse throughout the material with a dramatic increase of stress. The transition from the linear elastic to the collapse regimes was typically observed at approximately 10%–12% engineering strain, while densification was not observed until very large engineering strains (more than 35%–40%). The compressive modulus of each sub-region and of the gradient scaffold itself (Figure 5(b)) was calculated as a linear regression in the linear elastic region, between the engineering strain values of 0.02 and 0.1.<sup>16,19</sup> The presence of HAp in the collagen matrix significantly

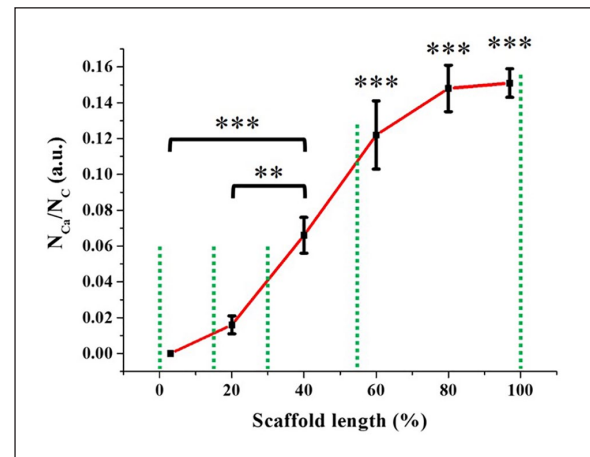


**Figure 4.** Gradient distribution of calcium atoms (i.e. HAp particles) throughout the scaffold ( $n=3$ ), from the cartilage-like region (0% of the scaffold length) to the bone-like region (100% of the scaffold length).

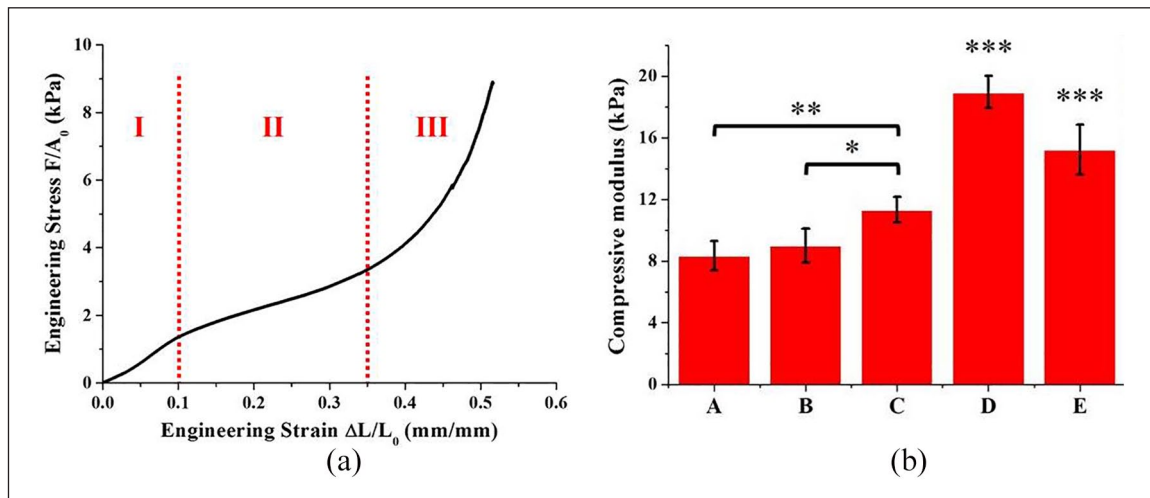


**Figure 5.** (a) Example of the engineering stress versus engineering strain curve obtained for each specimen in the uniaxial unconfined compression tests in wet state.  $F$  (mN) was the applied load,  $A_0$  ( $\text{mm}^2$ ) the initial value of the cross-sectional area of the specimen,  $\Delta L$  (mm) the displacement and  $L_0$  (mm) the initial height of the specimen. (b) Compressive moduli of the different sub-regions of the gradient scaffold and of the gradient scaffold itself ( $n=6$ ). The gradient distribution of HAp determined a gradient of stiffness in the scaffold: (A) cartilage-like region, (B) upper middle zone, (C) lower middle zone, (D) bone-like region and (E) gradient scaffold.

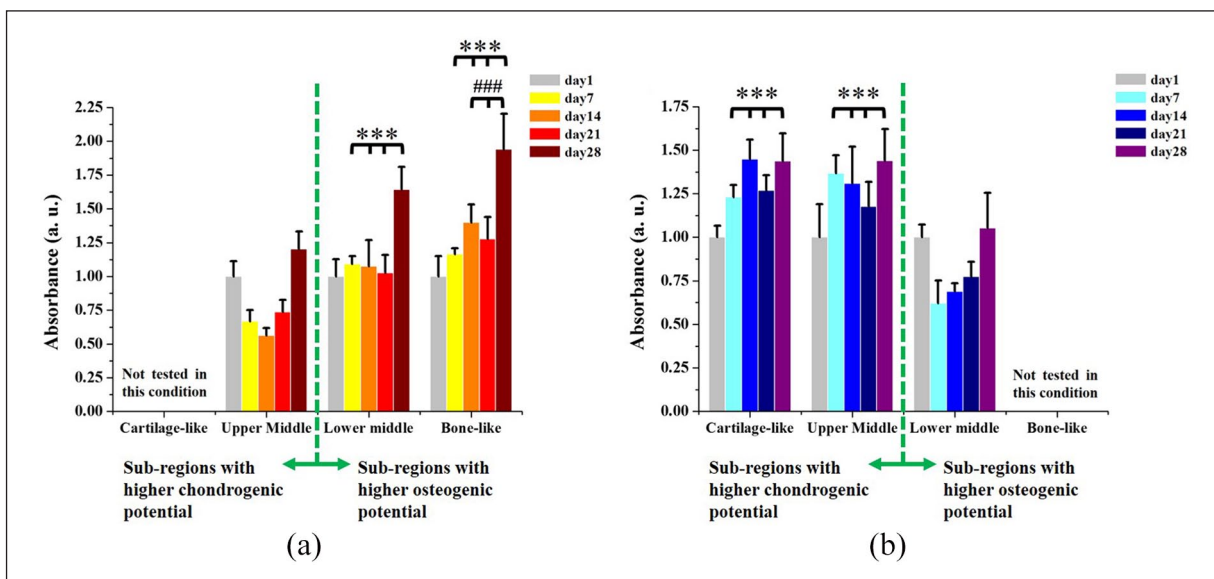


**Figure 6.** (a) Proliferation of hBMSCs in osteogenic differentiation medium increased with the increase of HAp content in the different sub-regions of the gradient scaffold ( $n=4$ ), due to the osteoinductive properties of its mineral phase: (\*) compared with upper middle zone at each time point and (#) compared with lower middle zone at each time point. (b) Proliferation of hBMSCs in chondrogenic differentiation medium increased in more chondrogenic sub-regions of the scaffold ( $n=4$ ): (\*) compared with the lower middle zone at each time point.

enhanced the mechanical properties of the material (Figure 5(b)). In particular, the compressive modulus of the different sub-regions of the gradient scaffold increased with the increasing HAp content. This result was in accordance with previous studies, which showed that the mechanical properties of collagen can be enhanced by adding a calcium phosphate phase.<sup>19,32</sup> Therefore, the designed gradient of stiffness for the scaffold was successfully obtained.

### Proliferation of hBMSCs

As shown in Figure 6(a), cell proliferation in osteogenic condition was significantly higher in the lower middle zone and in the bone-like region of the scaffold, compared with the upper middle zone, at each time point. The higher cell proliferation in osteogenic condition was expected, considering the higher concentration of the osteoconductive HAp in these regions.<sup>21</sup> A statistical difference was also observed in cell proliferation at day 14, day 21 and day 28 between bone-like region and lower middle zone. Similarly, cell proliferation when cells were cultured in chondrogenic condition was significantly higher in the cartilage-like region and in the upper middle zone of the gradient scaffold, compared with the lower middle zone, at each time point (Figure 6(b)).

Results obtained in both osteogenic and chondrogenic conditions confirmed that the gradient scaffold was able to selectively induce cell proliferation towards different lineages when cells were cultured in appropriate conditions.

The scaffold imparted a selective cue to the cells; gradient composition and stiffness directed and influenced cell proliferation, depending on the different sub-regions and whether it was more osteogenic or chondrogenic in nature. As expected, regions with a higher HAp content and stiffness favoured cell activity in osteogenic condition, due to the osteoconductive properties of calcium phosphates and due to the fact that a substrate with a higher stiffness can favour osteogenic differentiation of MSCs.<sup>21,33,34</sup> Regions with a higher content of chondrogenic collagen and a lower stiffness substrate favoured cell proliferation in chondrogenic condition.<sup>22,33,34</sup>

### In vivo biocompatibility

H&E staining, showed the gradient scaffold was significantly colonised by host cells after 15 days. A highly stromal fibrous-looking tissue containing many cells was observed (Figure 7). The tissue appeared healthy and highly vascularised with no evidence of inflammatory foreign body reaction. Cells were observed lining the scaffold forming perichondrium-like biomembrane with numerous small vessels in the vicinity (Figure 7). We speculate that this could be the beginning of perichondrium/ostium formation, which when fully matured and vascularised becomes the periosteum. The potential for the scaffold to drive differentiation potential was evaluated with immunohistochemistry and confirmed the presence of osteopontin,<sup>35</sup> an intracellular glycoprotein expressed in cells of the osteoblastic lineage and an indicator of osteoblast differentiation



(Figure 8(a)). Haematoxylin–Van Geisen stain for collagen was also positive indicating a potential differentiation towards the chondrogenic lineage (Figure 8(b)). MEF2C, a

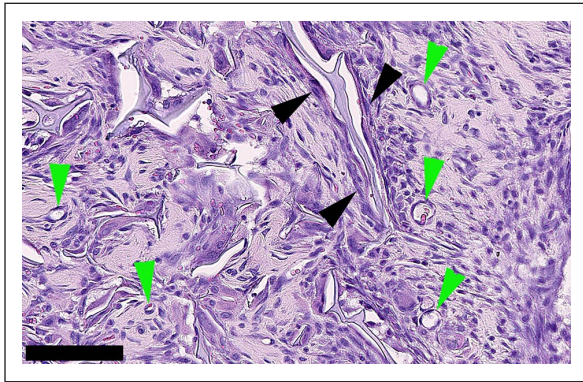


**Figure 7.** H&E staining of cells colonising the gradient scaffold. Scaffold and surrounding tissue were explanted after 15 days of subcutaneous implantation in rats. A highly stromal-looking tissue containing many spindle-shaped cells that appear to be fibroblastic was observed. The tissue appears highly vascularised (green arrowheads). Cells appear to be lining the scaffold in some areas (black arrow heads) which could be indicative of a perichondrium formation, with visible small blood vessels. Scale bar: 100  $\mu\text{m}$ .

potential osteoblast transcription factor,<sup>36</sup> was also expressed (Figure 8(c)). Cells in close contact with the scaffold had a homogeneous morphology and showed minimal inflammatory response, indicating that the scaffold was biocompatible (Figure 8(d)).

## Discussion

The development of an osteochondral tissue engineered scaffold, with the capacity to mimic the natural complex interface tissue, would be a major step forward for treating osteochondral defects. Recently, research is being directed towards scaffolds that aim to re-establish tissue–tissue interaction and allow a more natural integration.<sup>7</sup> To meet this need, this study used the ‘learning-from-nature’ approach to design and fabricate a continuous collagen matrix incorporating a gradient mineral phase, by inclusion of HAp particles, directly nucleated onto collagen fibres. The resultant scaffold has, therefore, a chemical gradient of an osteoinductive material, low-crystalline HAp, in a continuous collagenous matrix and a physical gradient of stiffness. Collagen molecules, acting as a template for HAp crystals, in a similar manner as in the natural process of biomineralisation, favoured the nucleation process and, consequently, prevented crystal

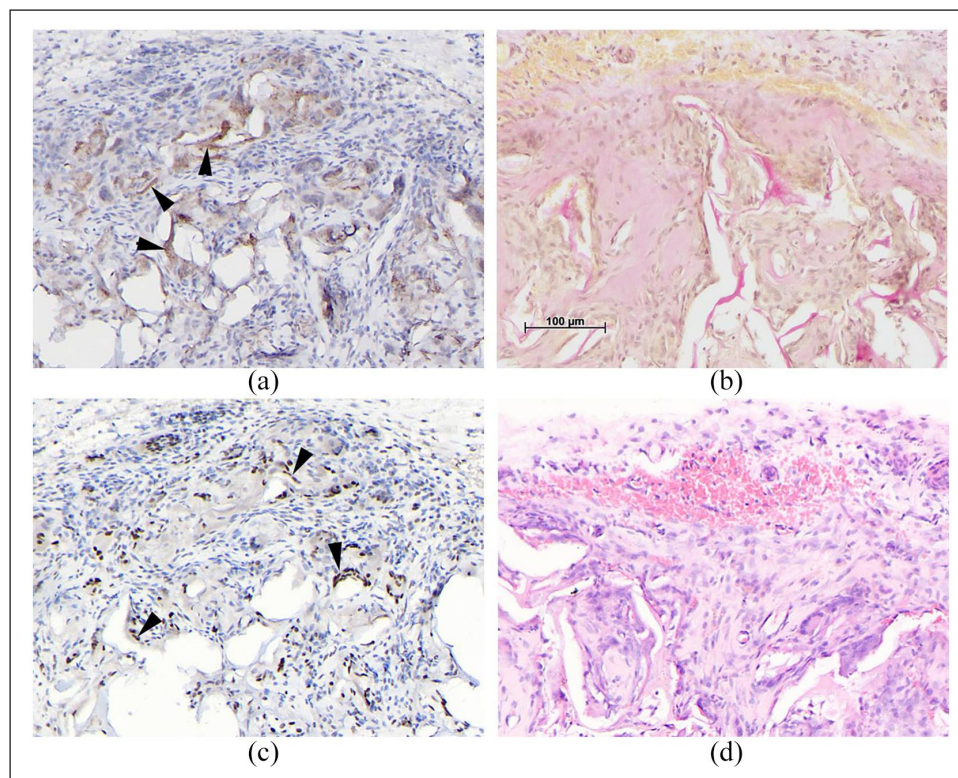


**Figure 8.** Representative images of subcutaneously implanted scaffold sections. Immunohistological staining for (a) osteopontin, arrows showing positive staining indicating presence of osteopontin. (b) HVG, identifying presence of collagen type I. (c) MEF2C, arrows indicate positive staining for this osteoblast transcription factor and (d) H&E showed minimal inflammatory response indicating the biocompatibility of the scaffold material. Scale bar = 100  $\mu\text{m}$  for all images.

growth, inducing the formation of low-crystalline apatite.<sup>37</sup> The well-documented osteogenic properties of HAp were then powered by a more physiological characteristic of this bioceramic, which has been demonstrated to be low-crystalline in natural immature bone tissue.<sup>29,30,38</sup> The advantage of a design including the direct nucleation of HAp particles onto the collagen fibres allowed the formation of low-crystalline HAp, in opposition to a direct addition of commercial HAp powder to a collagenous or, in general, polymeric matrix.<sup>37,39,40</sup> The fabrication process also allowed collagen and HAp to chemically integrate with each other. This interaction is fundamental to assure a chemical stability of the scaffold during its potential use for the regeneration of the damaged osteochondral tissue.

The designed gradient distribution of the mineral phase created a consequent gradient distribution of stiffness of the scaffold. The compressive modulus of the different sub-regions of the gradient scaffold increased progressively with the increasing of HAp content, from a softer collagenous cartilage-like region to a stiffer mineralised bone-like region. The gradient of stiffness was designed to drive cell behaviour by a physical signalling. It has been shown by several studies how the stiffness of the substrate can induce stem cell differentiation towards chondrocytes or osteoblasts lineage.<sup>33,41,42</sup> In particular, a lower stiffness substrate can favour differentiation towards soft tissue lineage, such as chondrogenic differentiation, whereas a higher stiffness substrate can promote osteogenic differentiation.<sup>34,41,43,44</sup>

As found in the biological evaluation with hBMSCs, the gradient of composition and stiffness favoured a more specific cell proliferation in the different selective sub-regions of the scaffold, according to their more chondrogenic or osteogenic potential. As expected, in regions with a higher HAp content and stiffness, cells showed higher proliferation in osteogenic medium. Chemical composition, that is, osteoinductivity, and physical composition, that is higher stiffness and signalling of HAp, increased cell proliferation, as already shown in the literature.<sup>21,37,45</sup> Similarly, in more collagenous regions characterised also by a lower stiffness substrate, cells showed higher proliferation in chondrogenic medium.<sup>22</sup> The design of the gradient scaffold successfully promoted cell activity in both the upper and sub-regions of the scaffold. The *in vivo* results demonstrated good biocompatibility, with minimal inflammatory response. The potential of the scaffold to selectively induce differentiation was demonstrated. Osteopontin, an intracellular glycoprotein expressed in cells of the osteoblastic lineage and an indicator of osteoblast differentiation,<sup>35</sup> was observed. Furthermore, the transcription factor MEF2C reported to be important in the development of several lineages including the regulation of skeletal tissues was also identified. This protein is known to be involved in vascular development and play a role in the development of cortical

architecture.<sup>36</sup> Collagen was also identified demonstrating the presence of connective tissue. While these markers are not confirmatory, and a more in-depth differentiation study is required, they are indicative that the scaffold has the potential to recruit cells and selectively induce differentiation of the recruited cells.

The continuous structure of the scaffold was created using a one-step freeze-drying process to obtain a highly porous gradient structure, without any discrete separations at the interfaces, and without the need for further processing to assure stable adhesion between different layers, as is commonly seen in the fabrication of multi-layered scaffolds. Layered scaffolds are fabricated comprising individual layers and are subsequently bonded together using specific agents, such as fibrin or other glues. Such discrete structure might induce an inhibition to cell migration at the interfaces between layers.<sup>2</sup> Another method that has been used for their fabrication is an iterative, multi-step freeze-drying process, where each layer is subsequently added to the others.<sup>6</sup> This fabrication process that requires multiple lyophilisation steps could be considered economically disadvantageous compared with the proposed one-step freeze-drying. The gradient scaffold proposed in this study was designed to generate a smooth transition between a hard and a soft tissue using bioactive and clinically approved biomaterials, namely, collagen and HAp, and a novel enhanced design, able to more closely mimic the unique natural osteochondral structure, using a more reproducible, efficient and economically advantageous fabrication process, which reduces the number of freeze-drying steps to just one and does not require any further treatment to avoid delamination or separation of the different layers. Moreover, the proposed fabrication process was designed to be easily coupled with medical imaging tools, such as 3D scans, to allow the production of custom-made (or 'patient-tailored') scaffolds. The reconstruction of the actual defect geometry by imaging tools (e.g. STL file) can be used to 3D-print the mould for the freeze-drying process. The inner cavity of the mould will be an exact replica of real geometry and dimensions of the patient's lesion. This will easily overcome the crucial limitation of reproducing irregular anatomical geometries for the fabrication of scaffolds for osteochondral tissue engineering. All these clear advantages of the proposed gradient scaffolds are summarised in Table 1, in a comparison of merits and demerits with other multi-layered or gradient scaffolds found in the literature.

## Conclusions

This study demonstrated the successful fabrication of a novel composite gradient scaffold with suitable biomimetic physicochemical and biological properties, for potential application in osteochondral regeneration. The scaffold was biomimetically designed to simulate the natural tissue

**Table 1.** Design of multi-layer or gradient scaffolds for osteochondral defects: brief overview of recent literature and comparison with proposed gradient scaffold (first row, italics).

Layers	Established gradients	Materials used	Fabrication methods	Limitations	Advantages	Ref.
NA	<ul style="list-style-type: none"> <li>• <i>Composition</i></li> <li>• <i>Stiffness</i></li> </ul>	<ul style="list-style-type: none"> <li>• <i>Collagen type I</i></li> <li>• <i>HAp</i></li> </ul>	<ul style="list-style-type: none"> <li>• <i>Freeze-drying</i></li> </ul>	<ul style="list-style-type: none"> <li>• <i>Material from animal origin (collagen)</i></li> <li>• <i>Isotropic structure</i></li> </ul>	<ul style="list-style-type: none"> <li>• <i>One-step processing</i></li> <li>• <i>Biomimetic materials</i></li> <li>• <i>Continuous integrated structure</i></li> <li>• <i>Solvent free</i></li> <li>• <i>Availability of custom-made design</i></li> </ul>	
3	<ul style="list-style-type: none"> <li>• Composition</li> <li>• Stiffness</li> </ul>	<ul style="list-style-type: none"> <li>• Gelatin</li> <li>• HAp</li> </ul>	<ul style="list-style-type: none"> <li>• Layer-by-layer freeze-drying</li> </ul>	<ul style="list-style-type: none"> <li>• Multi-step processing</li> </ul>	<ul style="list-style-type: none"> <li>• Continuous integrated structure</li> </ul>	Amadori et al. <sup>4</sup>
3	<ul style="list-style-type: none"> <li>• Composition</li> <li>• Porosity</li> <li>• Stiffness</li> </ul>	<ul style="list-style-type: none"> <li>• PLA</li> <li>• Sulphated cellulose nanocrystals</li> <li>• Phosphated cellulose nanocrystals</li> </ul>	<ul style="list-style-type: none"> <li>• Thermally induced phase separation</li> </ul>	<ul style="list-style-type: none"> <li>• Multi-step processing</li> <li>• Use of solvents for layer bonding</li> </ul>	<ul style="list-style-type: none"> <li>• Continuous integrated structure</li> <li>• Anisotropic structure</li> </ul>	Camarero-Espinosa et al. <sup>5</sup>
4	<ul style="list-style-type: none"> <li>• Composition</li> <li>• Porosity</li> <li>• Stiffness</li> </ul>	<ul style="list-style-type: none"> <li>• Collagen type I</li> <li>• Collagen type II</li> <li>• Hyaluronic acid</li> <li>• HAp</li> </ul>	<ul style="list-style-type: none"> <li>• Layer-by-layer freeze-drying</li> </ul>	<ul style="list-style-type: none"> <li>• Multi-step processing</li> </ul>	<ul style="list-style-type: none"> <li>• Continuous integrated structure</li> </ul>	Levingstone et al. <sup>6</sup>
4	<ul style="list-style-type: none"> <li>• Pore shape</li> </ul>	<ul style="list-style-type: none"> <li>• PCL</li> </ul>	<ul style="list-style-type: none"> <li>• Extrusion-based 3D printing</li> </ul>	<ul style="list-style-type: none"> <li>• No biomimetic materials</li> </ul>	<ul style="list-style-type: none"> <li>• Continuous integrated structure</li> </ul>	Di Luca et al. <sup>9</sup>
7	<ul style="list-style-type: none"> <li>• Composition</li> <li>• Stiffness</li> </ul>	<ul style="list-style-type: none"> <li>• PCL microspheres</li> <li>• HAp</li> </ul>	<ul style="list-style-type: none"> <li>• Layer-by-layer selective laser sintering</li> </ul>	<ul style="list-style-type: none"> <li>• Multi-step processing</li> </ul>	<ul style="list-style-type: none"> <li>• Continuous integrated structure</li> <li>• Microspheres for growth factor release</li> </ul>	Du et al. <sup>46</sup>
NA	<ul style="list-style-type: none"> <li>• Composition</li> <li>• Stiffness</li> </ul>	<ul style="list-style-type: none"> <li>• PLGA microspheres</li> <li>• Tricalcium phosphate</li> </ul>	<ul style="list-style-type: none"> <li>• Opposing syringes + freeze-drying</li> </ul>	<ul style="list-style-type: none"> <li>• Multi-step processing</li> </ul>	<ul style="list-style-type: none"> <li>• Continuous integrated structure</li> <li>• Microspheres for growth factor release</li> </ul>	Mohan et al. <sup>10,11</sup>
3	<ul style="list-style-type: none"> <li>• Composition</li> <li>• Porosity</li> </ul>	<ul style="list-style-type: none"> <li>• PLGA</li> <li>• PLGA microspheres</li> <li>• Chondroitin sulphate GMA</li> <li>• Gelatin GMA</li> </ul>	<ul style="list-style-type: none"> <li>• Particle leaching</li> <li>• UV crosslinking</li> </ul>	<ul style="list-style-type: none"> <li>• Multi-step processing</li> <li>• Discontinuous structure at the interface</li> </ul>	<ul style="list-style-type: none"> <li>• Microspheres for growth factor release</li> </ul>	Han et al. <sup>47</sup>

HAp: hydroxyapatite; PLA: polylactic acid; PCL: polycaprolactone; PLGA: poly(lactic-co-glycolic) acid; GMA: glycidyl methacrylate; UV: ultraviolet.

structure; a collagen matrix partially mineralised with HAp in its osteogenic sub-regions. The novel aspect was the creation of a continuous structure with a chemical gradient of a highly osteoinductive material (HAp), which imparted a physical gradient of stiffness with biomimetic functionality. Furthermore, this was achieved adopting an efficient and economically advantageous fabrication process. The gradient scaffold showed favourable biological potential both in vitro and in vivo. In vitro biological studies of the scaffold in presence of hBMSCs indicated the ability of cells to be directed by the chondrogenic or osteogenic environment created by the gradient material composition and stiffness in the different regions of the gradient scaffold. At the in vivo level, the biocompatibility of the gradient scaffold was confirmed by the subcutaneous implantation in rats, with minimal inflammatory response observed and evidence of cellular differentiation. The physicochemical properties of the gradient scaffold confirm its suitability for

use as an osteochondral graft for tissue regeneration. Both in vitro and in vivo biological evaluations show good biocompatibility with minimal inflammatory response. The in vivo study suggests that the scaffold has potential to selectively differentiate recruited cells, but confirmation is required with a more in-depth study.

### Acknowledgements

C.P. was involved in all experimental design, testing, analysis and interpretation of the acquired data. L.S. was involved in the development of the study design and in the interpretation of the results obtained. L.V. was involved in testing and interpretation of the biological data. M.P.S. and C.H. were involved in testing and interpretation of the data from the in vivo study. M.M. was involved in all analysis and interpretation of the data. A.S. was involved in the experimental design and interpretation of the acquired data. L.D.S. was involved in the experimental design, testing, analysis and interpretation of the acquired data.

## Declaration of conflicting interests

The author(s) declared no potential conflicts of interest with respect to the research, authorship and/or publication of this article.

## Funding

The author(s) disclosed receipt of the following financial support for the research, authorship and/or publication of this article: This project was partially funded by the Italian Ministry of Education, University and Research (MIUR) within the research grant PON02\_00563\_3448479 and the Dental Institute, King's College, London.

## ORCID iDs

Cristian Parisi  <https://orcid.org/0000-0002-6242-3784>

Lucy Di Silvio  <https://orcid.org/0000-0003-2554-2052>

## References

- Kim IL, Mauck RL and Burdick JA. Hydrogel design for cartilage tissue engineering: a case study with hyaluronic acid. *Biomaterials* 2011; 32(34): 8771–8782.
- Gadjanski I and Vunjak-Novakovic G. Challenges in engineering osteochondral tissue grafts with hierarchical structures. *Expert Opin Biol Ther* 2015; 15(11): 1583–1599.
- Nukavarapu SP and Dorcemus DL. Osteochondral tissue engineering: current strategies and challenges. *Biotechnol Adv* 2013; 31(5): 706–721.
- Amadori S, Torricelli P, Panzavolta S, et al. Multi-layered scaffolds for osteochondral tissue engineering: in vitro response of co-cultured human mesenchymal stem cells. *Macromol Biosci* 2015; 15(11): 1535–1545.
- Camarero-Espinosa S, Rothen-Rutishauser B, Weder C, et al. Directed cell growth in multi-zonal scaffolds for cartilage tissue engineering. *Biomaterials* 2016; 74: 42–52.
- Levingstone TJ, Ramesh A, Brady RT, et al. Cell-free multi-layered collagen-based scaffolds demonstrate layer specific regeneration of functional osteochondral tissue in caprine joints. *Biomaterials* 2016; 87: 69–81.
- Di Luca A, Van Blitterswijk C and Moroni L. The osteochondral interface as a gradient tissue: from development to the fabrication of gradient scaffolds for regenerative medicine. *Birth Defects Res C Embryo Today* 2015; 105(1): 34–52.
- Sridharan B, Mohan N, Berkland CJ, et al. Material characterization of microsphere-based scaffolds with encapsulated raw materials. *Mater Sci Eng C Mater Biol Appl* 2016; 63: 422–428.
- Di Luca A, Lorenzo-Moldero I, Mota C, et al. Tuning cell differentiation into a 3D scaffold presenting a pore shape gradient for osteochondral regeneration. *Adv Healthc Mater* 2016; 5(14): 1753–1763.
- Mohan N, Dormer NH, Caldwell KL, et al. Continuous gradients of material composition and growth factors for effective regeneration of the osteochondral interface. *Tissue Eng Part A* 2011; 17(21–22): 2845–2855.
- Mohan N, Gupta V, Sridharan BP, et al. Microsphere-based gradient implants for osteochondral regeneration: a long-term study in sheep. *Regen Med* 2015; 10(6): 709–728.
- Marrella A, Aiello M, Quarto R, et al. Chemical and morphological gradient scaffolds to mimic hierarchically complex tissues: from theoretical modeling to their fabrication. *Biotechnol Bioeng* 2016; 113(10): 2286–2297.
- Bailey BM, Nail LN and Grunlan MA. Continuous gradient scaffolds for rapid screening of cell-material interactions and interfacial tissue regeneration. *Acta Biomater* 2013; 9(9): 8254–8261.
- Haugh MG, Jaasma MJ and O'Brien FJ. The effect of dehydrothermal treatment on the mechanical and structural properties of collagen-GAG scaffolds. *J Biomed Mater Res A* 2009; 89(2): 363–369.
- Yannas IV. Collagen and gelatin in the solid state. *J Macromol Sci C* 1972; 7(1): 49–106.
- Harley BA, Leung JH, Silva EC, et al. Mechanical characterization of collagen-glycosaminoglycan scaffolds. *Acta Biomater* 2007; 3(4): 463–474.
- Salvatore L, Madaghiele M, Parisi C, et al. Crosslinking of micropatterned collagen-based nerve guides to modulate the expected half-life. *J Biomed Mater Res A* 2014; 102(12): 4406–4414.
- Best S and Bonfield W. Processing behaviour of hydroxyapatite powders with contrasting morphology. *J Mater Sci Mater Med* 1994; 5(8): 516–521.
- Kane RJ and Roeder RK. Effects of hydroxyapatite reinforcement on the architecture and mechanical properties of freeze-dried collagen scaffolds. *J Mech Behav Biomed Mater* 2012; 7: 41–49.
- Zhang Y, Hao L, Savalani MM, et al. In vitro biocompatibility of hydroxyapatite-reinforced polymeric composites manufactured by selective laser sintering. *J Biomed Mater Res A* 2009; 91(4): 1018–1027.
- Woodard JR, Hilldore AJ, Lan SK, et al. The mechanical properties and osteoconductivity of hydroxyapatite bone scaffolds with multi-scale porosity. *Biomaterials* 2007; 28(1): 45–54.
- Zhou J, Xu C, Wu G, et al. In vitro generation of osteochondral differentiation of human marrow mesenchymal stem cells in novel collagen-hydroxyapatite layered scaffolds. *Acta Biomater* 2011; 7(11): 3999–4006.
- Bonnier F, Keating ME, Wróbel TP, et al. Cell viability assessment using the alamar blue assay: a comparison of 2D and 3D cell culture models. *Toxicol in Vitro* 2015; 29(1): 124–131.
- Domingos M, Gloria A, Coelho J, et al. Three-dimensional printed bone scaffolds: the role of nano/micro-hydroxyapatite particles on the adhesion and differentiation of human mesenchymal stem cells. *Proc IMechE Part H: J Engineering in Medicine* 2017; 231(6): 555–564.
- Salifu AA, Lekakou C and Labeed F. Electrospun oriented gelatin-hydroxyapatite fiber scaffolds for bone tissue engineering. *J Biomed Mater Res A* 2017; 105(7): 1911–1926.
- Parisi C, Gervaso F, Scalera F, et al. Influence of the precipitation temperature on properties of nanohydroxyapatite powder for the fabrication of highly porous bone scaffolds. *Key Eng Mater* 2014; 587: 27–32.
- Müller WEG, Tolba E, Schroder HC, et al. Amorphous polyphosphate-hydroxyapatite: a morphogenetically active substrate for bone-related SaOS-2 cells in vitro. *Acta Biomater* 2016; 31: 358–367.

28. Al-Munajjed AA, Plunkett NA, Gleeson JP, et al. Development of a biomimetic collagen-hydroxyapatite scaffold for bone tissue engineering using a SBF immersion technique. *J Biomed Mater Res B Appl Biomater* 2009; 90(2): 584–591.
29. Miller LM, Vairavamurthy V, Chance MR, et al. In situ analysis of mineral content and crystallinity in bone using infrared micro-spectroscopy of the  $\nu_4$   $\text{PO}_4^{3-}$  vibration. *BBA-Gen Subjects* 2001; 1527(1–2): 11–19.
30. Xia Z, Yu X, Jiang X, et al. Fabrication and characterization of biomimetic collagen-apatite scaffolds with tunable structures for bone tissue engineering. *Acta Biomater* 2013; 9(7): 7308–7319.
31. Zhang W, Huang Z-L, Liao S-S, et al. Nucleation sites of calcium phosphate crystals during collagen mineralization. *J Am Ceram Soc* 2003; 86(6): 1052–1054.
32. Gleeson JP, Plunkett NA and O'Brien FJ. Addition of hydroxyapatite improves stiffness, interconnectivity and osteogenic potential of a highly porous collagen-based scaffold for bone tissue regeneration. *Eur Cell Mater* 2010; 20: 218–230.
33. Lv H, Li L, Sun M, et al. Mechanism of regulation of stem cell differentiation by matrix stiffness. *Stem Cell Res Ther* 2015; 6: 103–111.
34. MacQueen L, Sun Y and Simmons CA. Mesenchymal stem cell mechanobiology and emerging experimental platforms. *J R Soc Interface* 2013; 10(84): 20130179.
35. Chen Q, Shou P, Zhang L, et al. An osteopontin-integrin interaction plays a critical role in directing adipogenesis and osteogenesis by mesenchymal stem cells. *Stem Cells* 2014; 32(2): 327–337.
36. Stephens AS, Stephens SR, Hobbs C, et al. Myocyte enhancer factor 2C, an osteoblast transcription factor identified by dimethyl sulfoxide (DMSO)-enhanced mineralization. *J Biol Chem* 2011; 286(34): 30071–30086.
37. Minardi S, Corradetti B, Taraballi F, et al. Evaluation of the osteoinductive potential of a bio-inspired scaffold mimicking the osteogenic niche for bone augmentation. *Biomaterials* 2015; 62: 128–137.
38. Farlay D, Panczer G, Rey C, et al. Mineral maturity and crystallinity index are distinct characteristics of bone mineral. *J Bone Miner Metab* 2010; 28(4): 433–445.
39. Chen J, Chen H, Li P, et al. Simultaneous regeneration of articular cartilage and subchondral bone in vivo using MSCs induced by a spatially controlled gene delivery system in bilayered integrated scaffolds. *Biomaterials* 2011; 32(21): 4793–4805.
40. Park S, Lee S and Kim W. Fabrication of porous polycaprolactone/hydroxyapatite (PCL/HA) blend scaffolds using a 3D plotting system for bone tissue engineering. *Bioprocess Biosyst Eng* 2011; 34(4): 505–513.
41. Steinmetz NJ, Aisenbrey EA, Westbrook KK, et al. Mechanical loading regulates human MSC differentiation in a multi-layer hydrogel for osteochondral tissue engineering. *Acta Biomater* 2015; 21: 142–153.
42. Wen JH, Vincent LG, Fuhrmann A, et al. Interplay of matrix stiffness and protein tethering in stem cell differentiation. *Nat Mater* 2014; 13(10): 979–987.
43. Engler AJ, Sen S, Sweeney HL, et al. Matrix elasticity directs stem cell lineage specification. *Cell* 2006; 126(4): 677–689.
44. Salamon A, van Vlierberghe S, van Nieuwenhove I, et al. Gelatin-based hydrogels promote chondrogenic differentiation of human adipose tissue-derived mesenchymal stem cells *in vitro*. *Materials* 2014; 7(2): 1342–1359.
45. Yan L-P, Silva-Correia J, Oliveira MB, et al. Bilayered silk/silk-nanoCaP scaffolds for osteochondral tissue engineering: in vitro and in vivo assessment of biological performance. *Acta Biomater* 2015; 12: 227–241.
46. Du Y, Liu H, Yang Q, et al. Selective laser sintering scaffold with hierarchical architecture and gradient composition for osteochondral repair in rabbits. *Biomaterials* 2017; 137: 37–48.
47. Han F, Zhou F, Yang X, et al. A pilot study of conically graded chitosan-gelatin hydrogel/PLGA scaffold with dual-delivery of TGF- $\beta$ 1 and BMP-2 for regeneration of cartilage-bone interface. *J Biomed Mater Res B Appl Biomater* 2015; 103(7): 1344–1353.